MOLEKUL
eISSN: 2503-0310
Articles
https://doi.org/10.20884/1.jm.2026.21.1.17837

Rice Husk Ash-Derived Magnetized Silica Functionalized with TMPDT for Heavy Metal Ion Removal

Sri Hastuti*, Hasna Haifa Irfani, Rifania Aura Nuzula, Teguh Endah Saraswati, Abu Masykur, Candra Purnawan, Atmanto Heru Wibowo, Dina Fitriana

Department of Chemistry, Faculty of Mathematics and Natural Sciences, Universitas Sebelas Maret, Jl. Ir. Sutami 36A Surakarta 57126, Indonesia

*Corresponding author email: srihastuti71@staff.uns.ac.id

Received September 27, 2025; **Accepted** February 22, 2026; **Available online** March 20, 2026

ABSTRACT. The removal of toxic heavy metal ions from water remains a critical environmental challenge. In this study, a novel magnetized mesoporous silica adsorbent functionalized with N1-(3-trimethoxysilylpropyl) diethylenetriamine (Fe_3O_4@SiO_2@meso-SiO2@TMPDT), synthesized from rice husk ash, was developed for the adsorption of Cd(II) and Pb(II) ions. The characterization of the adsorbent by FTIR, SEM-EDX, and TGA confirmed the successful synthesis of magnetized and TMPDT-functionalized silica derived from rice husk ash (Fe_3O_4@SiO_2@meso-SiO_2@TMPDT). The adsorption study consists of the determination of optimum pH, the adsorption kinetics study, and the adsorption isotherm. Batch adsorption studies showed that the optimal pH values for Cd(II) and Pb(II) adsorption were 4 and 3, respectively. The adsorption kinetics for both metal ions followed a pseudo-second-order model. Furthermore, the adsorption isotherms fitted both the Langmuir and the Freundlich models with comparable R^2 values. The maximum adsorption capacities (Q_m) of Fe_3O_4@SiO_2@meso-SiO_2@TMPDT for Cd(II) and Pb(II) were 28.089 and 24.498 mg/g, respectively. These findings demonstrate that the developed adsorbents offer an effective and sustainable approach for heavy metal removal from aqueous systems.

Keywords: adsorption, heavy metal ions, magnetized silica, rice husk ash, TMPDT

INTRODUCTION

Clean water is a basic human necessity and plays a crucial role in supporting public health and sustainable development. However, water resources are increasingly threatened by various pollutants, particularly heavy metals such as cadmium (Cd(II)) and lead (Pb(II)), which are known for their toxicity and persistence in the environment. Cadmium is easily absorbed through the respiratory system and has been identified as a carcinogen that impacts the prostate, lungs, pancreas, and urinary tract (Fitriana et al., 2025).

To mitigate heavy metal pollution, the development of effective and environmentally friendly adsorbent materials has become a focus of recent research. Many organic waste materials were used to reduce the concentration of toxic pollutants in an aqueous medium, for example, rice husk. Rice husk is an abundant agricultural byproduct in Indonesia that is frequently discarded or incinerated, which contributes to carbon emissions and air pollution. Due to its significant amount of silica (SiO_2), about 15-20% by weight, rice husk is a promising alternative source of silica for material synthesis (Sakti et al., 2013). Additionally, it consists of 60% volatile matter, 15% carbon, and 5% ash content (Priya et al., 2022).

Silica derived from rice husk ash has been utilized in various applications, including nanoparticle synthesis (El-Said et al., 2018; Larkunthod et al., 2022) and organic modification (Hastuti et al., 2019; Martini et al., 2024; Montalvo-Andía et al., 2022). However, the adsorption performance of raw or non-porous silica remains limited due to its relatively low surface area and restricted accessibility of active sites.

To overcome these limitations, silica can be engineered into mesoporous structures using surfactants such as cetyltrimethylammonium bromide (CTAB), which significantly enhance surface area, pore volume, and the density of surface silanol groups (Awual et al., 2014; Kheshti & Hassanajili, 2017).

Mesoporous silica is an excellent material for adsorption because of its high surface area, pore size control, and high concentration of surface silanol (Si-OH) groups. However, a major challenge in practical wastewater treatment lies in the recovery and reuse of fine adsorbent particles. Additionally, the synthesis of mesoporous silica is cost-effective and non-toxic (Cheng et al., 2025). These characteristics make mesoporous silica ideal for applications such as adsorption (Awual et al., 2014; He et al., 2024), catalysis (Mayoral et al., 2013), separation (Ripon et al., 2024), (Ripon et al., 2024), and nanomaterial storage (Narayan et al., 2018; Sanjay et al., 2018; Varache et al., 2019).

Magnetic modification of silica using magnetite (Fe_3O_4), an emerging wastewater treatment technology, offers advantages such as efficient recovery and reuse through external magnetic separation (Liu et al., 2016). Several studies have developed magnetic silica-based materials, such as magnetic ion-imprinted polymers for Cu(II) (Zhan et al., 2011), silica-coated magnetite composites (Husain et al., 2019), and magnetic materials modified with organic ligands of L-arginine and diethylenetriamine (Amaria et al., 2017; Fahmiati et al., 2018; Jiaqi et al., 2019).

Moreover, recent research has shown that the mesoporous silica functionalized with different groups, such as thiol, phenol, carboxyl, or amine groups, can improve the adsorption capacity and selectivity. For instance, silica functionalized with amine, sulfonic, or thiocyanate groups (Beagan et al., 2022), carboxyl-functionalized SBA-15 and SBA-16 mesoporous silica (Yu et al., 2025), multifunctional hybrid silica (Javaheri et al., 2019), and FeMnOx/SBA-15 (Zhou et al., 2020) have demonstrated promising adsorption capabilities. It has been found that functional groups such as diethylenetriamine, 3-aminopropyltrimethoxysilane, and N-[3-(trimethoxysilyl)propyl] diethylenetriamine (TMPDT) also significantly enhance the adsorption capacity (Beagan et al., 2022; Chan et al., 2011; Hastuti et al., 2025). The presence of multiple amine groups, which provide strong binding affinity toward metal ions, makes TMPDT very useful.

However, the integration of TMPDT-functionalized mesoporous silica derived from rice husk ash with magnetic Fe_3O_4 cores for the removal of Cd(II) and Pb(II) remains insufficiently explored. A multifunctional adsorbent with a high surface area, improved selectivity, and superior separation performance is produced by combining a superparamagnetic Fe_3O_4 core, a mesoporous silica shell, and TMPDT functionalization. Furthermore, this study aims to synthesize and characterize a TMPDT-functionalized magnetized mesoporous silica derived from rice husk ash for Cd(II) and Pb(II) ions removal. The uniqueness of this work lies in the combination of sustainable biomass-derived silica, magnetic separability, and amine-rich functionalization within a single adsorbent system for Cd(II) and Pb(II) removal.

EXPERIMENTAL SECTION

Materials

Magnetite (Fe_2O_3) was purchased from China (technical grade). Sodium hydroxide (NaOH), ethanol (C_2H_5OH), ammonia solution (NH_4OH), cetyltrimethylammonium bromide (CTAB), toluene, acetone, hydrochloric acid (HCl) (purity 37%), lead nitrate ($Pb(NO_3)_2$), cadmium nitrate ($Cd(NO_3)_2$), and N'-(3-trimethoxysilylpropyl)diethylenetriamine (TMPDT) were purchased from Merck with pure analysis quality.

The instruments used in this study included an Atomic Absorption Spectrophotometer (AAS, Shimadzu model AA-6650F), a Fourier Transform Infrared Spectrophotometer (FTIR, Shimadzu IR Prestige-21), a Scanning Electron Microscope with Energy Dispersive X-ray detector (SEM-EDX, Quanta 400 FEG A), and *Simultaneous Thermal Analyzer* (STA Linseis PT1600).

The Synthesis of Fe_3O_4@SiO_2@meso-SiO_2 Adsorbent

Synthesis of sodium silicate (Na_2SiO_3)

The preparation of Na_2SiO_3 was carried out based on the methods outlined by Hastuti et al. (2019) and Sakti et al. (2013). 160 mL of a 4M NaOH solution was mixed with 20 g of rice husk ash. The mixture was heated to 60 to 80 °C while being agitated to thicken it. After that, the viscous mixture was calcined at 500 °C in a furnace for 30 minutes. The resultant solid was cooled, submerged in 200 mL of distilled water, and filtered. The sodium silicate (Na_2SiO_3) was the filtrate that was obtained.

Synthesis of Fe_3O_4@SiO_2

The synthesis of Fe_3O_4@SiO_2 was carried out based on the method reported by Kheshti et al. (2019) with some modifications. 0.4 g of Fe_3O_4 was dispersed in 10 mL of distilled water, which was then sonicated for 30 minutes. After that, 15 mL of Na_2SiO_3 was added while being constantly stirred, and then 4 M HCl was added dropwise till gel formation was observed. The resultant gel was allowed to stand overnight, then washed with distilled water until a neutral pH, then dried in an oven.

Synthesis of Fe_3O_4@SiO_2@meso-SiO_2

Mixture A: 0.1 g of Fe_3O_4@SiO_2 was dispersed in 10 mL of distilled water, then sonicated for 10 minutes. Next, different amounts of Na_2SiO_3 (1, 3, and 5 mL) were added. Mixture B: 0.3 g of CTAB was dispersed in 40 mL of distilled water, then sonicated for 10 minutes. Mixture A was then combined with Mixture B, stirred for 6 hours, and adjusted with 4 M HCl until a gel was formed. The resulting gel was dried in an oven at 60 °C, then 2 g of the product was added to 100 mL of ethanol containing 2% ammonium nitrate, then refluxed for 1 hour at room temperature. The product was dried in an oven at 60 °C, then calcined in a furnace at 300 °C for 3 hours.

Synthesis of Fe_3O_4@SiO_2@meso-SiO_2@TMPDT

A total of 0.5 h of Fe_3O_4@SiO_2@meso-SiO_2 was dispersed in 70 mL of toluene, then sonicated for 30 minutes. After that, 2 mL of TMPDT was added to the mixture, which was then refluxed at 110°C for 24 hours. The resulting material was washed with ethanol and acetone, followed by drying in an oven at 60 °C for 12 hours.

The Adsorption of Cd(II) and Pb(II) Ions on Fe_3O_4@SiO_2@meso-SiO_2@TMPDT

pH optimization

To investigate the effect of pH on the adsorption of Cd(II) and Pb(II) metal ions, 0.01 g of

$Fe_3O_4@SiO_2@meso\text{-}SiO_2@TMPDT$ as initial adsorbent dosage is added to 10 mL of 10 mg. L^{-1} of metal ions, the pH was measured from 3.0 to 8.0. The mixtures were agitated using a shaker for 1 hour. The solid adsorbent was then separated using a magnet and filtered through Whatman No. 42 filter paper. The calculated values of the experiment results were based on the results obtained from duplicate measurements. The results of the two repetitions showed no significant difference, as indicated by the very small error bar values on the graph.

Adsorption kinetics studies

A total of 0.01 g of $Fe_3O_4@SiO_2@meso\text{-}SiO_2@TMPDT$ was added to 10 mL of 10 mg.L^{-1} of metal ions, and the adsorption process was conducted over varying contact times of 0, 10, 20, 30, 40, 50, 60, and 90 minutes at the optimum pH. The data collected from these experiments were utilized to analyze the adsorption kinetics by fitting the results to various kinetic models, including first order (Eq. 1), second order (Eq. 2), pseudo-first-order (Eq. 3), and pseudo-second-order (Eq. 4) models.

$$\ln C_A = -kt + C_0 \tag{1}$$

$$\frac{1}{C_A} - \frac{1}{C_{A_0}} = kt \tag{2}$$

$$\ln(q_e - q_t) = \ln q_e - k_1 t \tag{3}$$

$$\frac{t}{q_t} = \frac{1}{k_2 q_e^2} + \frac{1}{q_e} t \tag{4}$$

where C_A and C_0 are the concentrations at time t and initial time (mg/L), respectively; k is the rate constant; t is the contact time (min); q_e and q_t are the adsorbed amounts at equilibrium and at time t (mg/g), respectively.

Adsorption isotherm studies

A total of 0.01 g of $Fe_3O_4@SiO_2@meso\text{-}SiO_2@TMPDT$ was added to 10 mL of Cd(II) solution at varying concentrations (5–30 ppm) under optimum pH. The suspensions were agitated at the optimum contact time using a mechanical shaker. Afterward, the mixtures were filtered, and the residual solids were separated with an external magnetic field. The filtrates were analyzed by AAS, and the data were fitted to the Langmuir (Eq. 5) and Freundlich (Eq. 6) isotherm models.

$$\frac{C_e}{Q_e} = \frac{1}{Q_m} C_e + \frac{1}{K_L Q_m} \tag{5}$$

$$\ln Q_e = ln\, K_F + \frac{1}{n} \ln C_e \tag{6}$$

where K_L and K_F are the Langmuir and the Freundlich constants, respectively, n is the heterogeneity factor, Q_m is the maximum adsorption capacity, and C_e is the equilibrium concentration (mg/L).

RESULTS AND DISCUSSION

The Characterization of $Fe_3O_4@SiO_2@mesoSiO_2@$ TMPDT

The material synthesis was carried out in stages, starting with the preparation of $Fe_3O_4@SiO_2$material, followed by the formation of meso-silica through the addition of varying volumes of Na_2SiO_3. The next step involved the addition of TMPDT to form the $Fe_3O_4@SiO_2@mesoSiO_2@TMPDT$ material. In the meso-silica formation stage, variations in the amount of Na_2SiO_3 were applied. This was done to evaluate the magnetic pull strength of the adsorbent material. A thicker meso-silica layer helps to enhance adsorption capacity, but it becomes more difficult to be magnetically pulled. Therefore, optimization of Na_2SiO_3 addition was carried out, and the results can be seen in the observation data presented in **Figure 1.**

Based on **Figure 1**, the variation in the Na_2SiO_3 volume led to materials with distinct physical and magnetic properties. The addition of 1 mL resulted in a material with a dark color, indicating a relatively thin meso-silica layer, while maintaining strong magnetic properties. In contrast, the addition of 5 mL produced a material with a whitish-gray appearance, suggesting a thicker meso-silica layer, but with reduced magnetic responsiveness. Based on these observations, the addition of 3 mL was selected, as it provided an adequate meso-silica layer while retaining strong magnetic properties. This combination offers potential advantages for more efficient metal ion separation. The meso-silica layer enhances the adsorption capacity, while the magnetic properties facilitate the effective separation of metal ions from solution. **Figure 2** presents a schematic representation of the synthesis of $Fe_3O_4@SiO_2@mesoSiO_2@TMPDT$ from rice husk ash for the adsorption of Cd(II) and Pb(II).

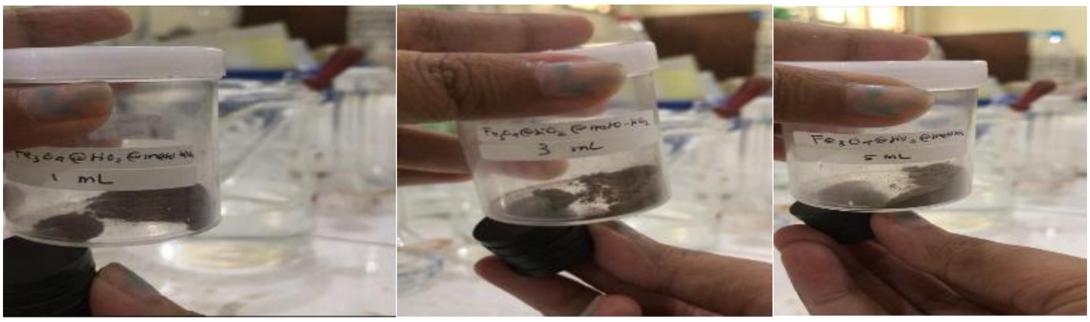

(a) (b) (c)

Figure 1. The effect of Na_2SiO_3 variations on the formation of $Fe_3O_4@SiO_2@mesoSiO_2$ (**a**) 1 ml, (**b**) 3 ml, and (**c**) 5 ml

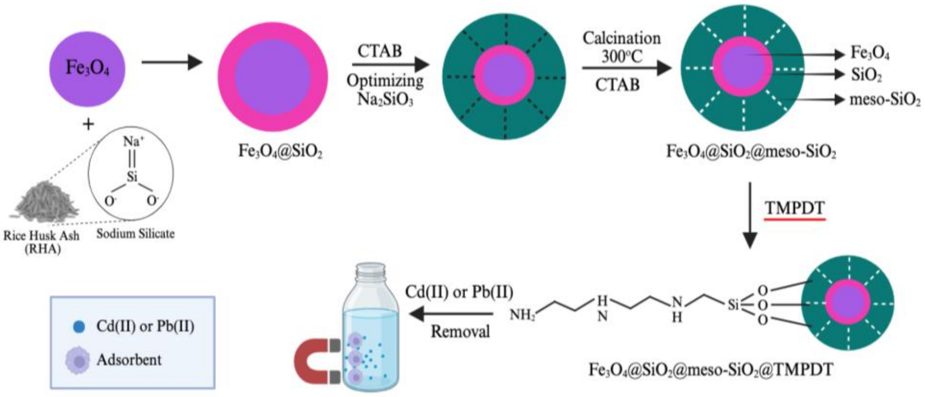

Figure 2. The schematic representation of the synthesis of $Fe_3O_4@SiO_2@meso\text{-}SiO_2@TMPDT$ for the adsorption of Cd(II)and Pb(II)

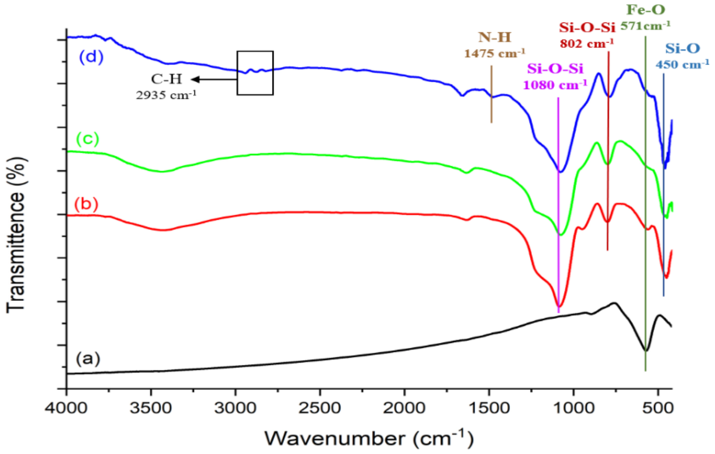

Figure 3. FTIR spectra of (**a**) Fe_3O_4, (**b**) $Fe_3O_4@SiO_2$, (**c**) $Fe_3O_4@SiO_2@meso\text{-}SiO_2$, (**d**) $Fe_3O_4@SiO_2@meso\text{-}SiO_2@TMPDT$

Figure 3 illustrates the FTIR spectra of Fe_3O_4, $Fe_3O_4@SiO_2$, $Fe_3O_4@SiO_2@meso\text{-}SiO_2$, and $Fe_3O_4@SiO_2@meso\text{-}SiO_2@TMPDT$. In the Fe_3O_4 material, an infrared absorption band was observed at 570.95 cm^{-1}, indicating the presence of Fe–O bonds (Bouafia et al., 2022). Further FTIR analysis revealed characteristic Si–O–Si symmetric stretching bands at 802.42 cm^{-1}, 805.32 cm^{-1}, and 786.03 cm^{-1} for $Fe_3O_4@SiO_2$, $Fe_3O_4@SiO_2@meso\text{-}SiO_2$, and $Fe_3O_4@SiO_2@meso\text{-}SiO_2@TMPDT$, respectively. Asymmetric Si–O–Si stretching was also identified at 1087 cm^{-1}, 1082 cm^{-1}, and 1083 cm^{-1} (Meng et al., 2016). In the $Fe_3O_4@SiO_2@meso\text{-}SiO_2@TMPDT$ material, additional distinct peaks were observed, confirming the successful functionalization with N′-(3 trimethoxysilylpropyl) diethylenetriamine (TMPDT). These include Si–C at 789.88 cm^{-1}, C–H bending at 2935.78 cm^{-1}, and N–H stretching at 1475.61 cm^{-1}. The presence of these functional groups confirms the successful attachment of TMPDT, thereby enhancing the material's potential as an adsorbent.

The surface morphology of the samples was analyzed using Scanning Electron Microscopy (SEM) to evaluate topographic changes resulting from the multilayer coating process. The SEM image of the $Fe_3O_4@SiO_2$ as presented in **Figure 4** (**a**) shows a surface dominated by a fine granular texture with the formation of relatively compact aggregates. In some areas, domains with higher contrast, rounded to polygonal in shape, are observed, indicating the presence of larger particles or aggregates embedded in the granular matrix.

In the $Fe_3O_4@SiO_2@meso\text{-}SiO_2@TMPDT$ (**Figure 4(b)**), the morphology changes to aggregates with a nodular character, characterized by rounded subunit boundaries and the presence of interdomain bridging structures. This increase in nodular texture and aggregate enlargement is consistent with the growth of additional silica layers ($meso\text{-}SiO_2$) and modification of interfacial interactions after TMPDT functionalization. These changes in surface properties have the potential to increase the tendency for agglomeration, particularly during the drying stage.

The SEM results confirm that the addition of the $meso\text{-}SiO_2$ layer and TMPDT functionalization contribute to an increase in the aggregate size and produce a rougher surface topography with a more pronounced nodular character.

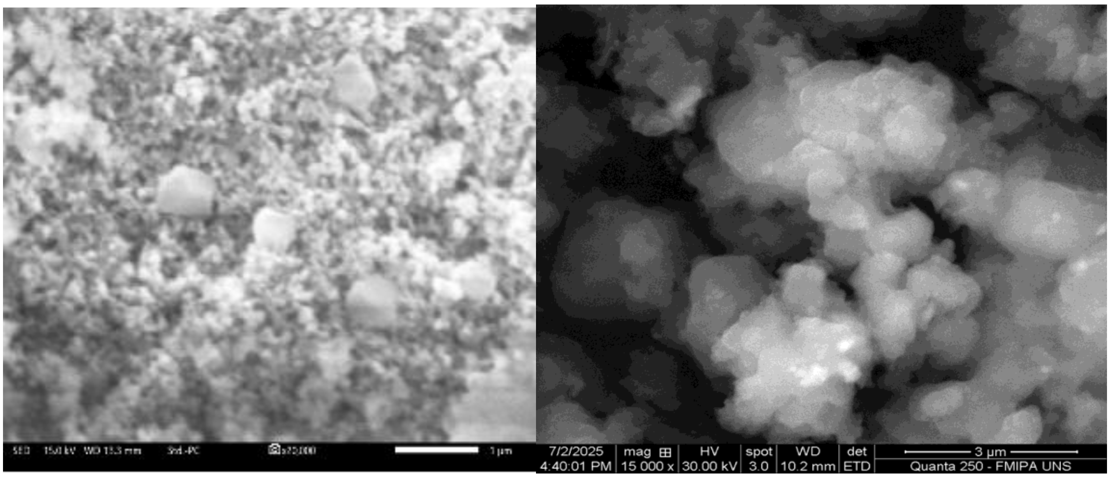

(a) (b)

Figure 4. SEM images of (**a**) Fe_3O_4@SiO_2 and (**b**) Fe_3O_4@SiO_2@meso-SiO_2@TMPDT

Table 1. EDX Elemental composition of Fe_3O_4@SiO_2 and Fe_3O_4@SiO_2@meso-SiO_2@TMPDT

Element	Weight (%)	
	Fe_3O_4@SiO_2	Fe_3O_4@SiO_2@meso-SiO_2@TMPDT
C	8.97	41.66
N	-	8.48
O	49.38	38.89
Si	28.16	10.56
Fe	-	0.41

SEM–EDX analysis was performed to assess changes in the elemental composition of the samples after the coating and functionalization processes. According to **Table 1**, the Fe_3O_4@SiO_2 sample is dominated by O (49.38 wt%) and Si (28.16 wt%), which is consistent with the formation of a silica layer/matrix on the surface. The measured C content is relatively low (8.97 wt%) and likely originates from small amounts of residual organic components, such as residues from rice husk ash-based silica sources. Under these measurement conditions, no Fe signal was detected, indicating that the analyzed area primarily represents the surface (shell) portion of the silica, thus masking the contribution of the Fe_3O_4 core and not detectable by EDX.

After the sample was modified to Fe_3O_4@SiO_2@meso-SiO_2@TMPDT, the C content increased sharply to 41.66 wt%, and the N content increased to 8.48 wt%. These findings indicate a more dominant organic component and support the successful functionalization using TMPDT. Concurrently, the Si mass fraction decreased from 28.16 to 10.56 wt%, and O decreased from 49.38 to 38.89 wt%. This decrease can be explained by the sample surface now being dominated by an organic layer, resulting in a smaller relative contribution of the silica phase in weight percent (wt%) calculations. Fe was detected at a very low level (0.41 wt%), confirming that the Fe_3O_4 core is still covered by the silica and organic layers, thus dampening the Fe signal, given EDX's greater sensitivity to surface composition. The EDX results support the successful addition of organic layers and functionalization.

Figure 5 presents the thermogravimetric analysis (TGA) profile of Fe_3O_4@SiO_2@meso-SiO_2@TMPDT, showing two distinct mass loss events occurring within the temperature ranges of 62–393 °C and 446–577 °C, corresponding to weight losses of 60.64% and 38.87%, respectively. The first mass loss (62–393 °C) is attributed to the release of physically adsorbed water (H_2O) and dehydration during the formation of siloxane bonds. This stage is also likely associated with the thermal decomposition of residual organic components, particularly the CTAB surfactant used during the synthesis of mesoporous silica. The second stage (446–577 °C) corresponds to the degradation of more thermally stable carbonaceous residues or organic fragments derived from TMPDT, indicating successful functionalization of the composite material. The observed thermal behavior is consistent with the findings of Kheshti and Hassanajili (2017), who reported that Fe_3O_4@SiO_2@meso-SiO_2–NH_2 materials exhibit initial mass loss below 180 °C due to water evaporation, followed by significant degradation of grafted organic groups in the 200–600 °C range.

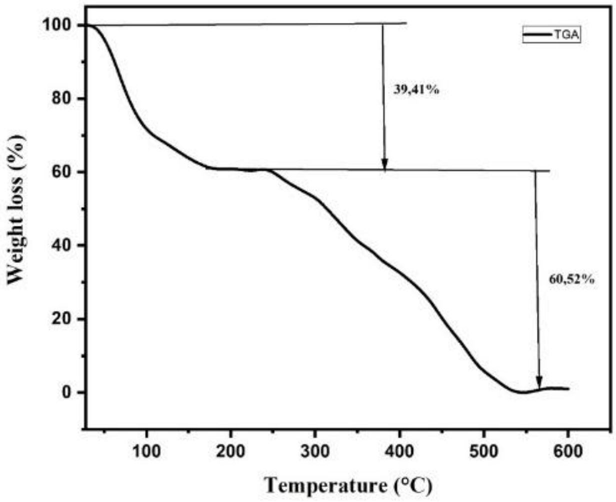

Figure 5. TGA analysis of $Fe_3O_4@SiO_2@meso\text{-}SiO_2@TMPDT$

The Adsorption of Cd(II) and Pb(II) Ions on $Fe_3O_4@SiO_2@meso\text{-}SiO_2@TMPDT$

Effect of pH on Cd(II) and Pb(II) removal

Figure 6 illustrates the effect of pH on the adsorption performance of TMPDT-functionalized magnetized silica. The adsorption capacity for Cd(II) increases with rising pH from 3 to a maximum at pH 5, followed by a gradual decrease up to pH 9. The enhanced adsorption at low pH up to pH 5 can be attributed to favorable electrostatic interactions between protonated amine groups ($-NH_3^+$) from TMPDT and the target Cd(II) ions in solution. At low pH, the high concentration of H^+ ions leads to a positively charged adsorbent surface, which causes electrostatic repulsion with the positively charged Cd(II) ions (Sanati et al., 2019).

Furthermore, as the pH increases, the deprotonation of the amine groups facilitates complexation or ligand coordination with Cd(II), enhancing binding affinity. The optimum adsorption capacity is achieved at pH 5, where these interactions reach an ideal balance. A higher concentration of hydroxide ions (OH^-) results in a decrease in adsorption capacity. This condition is probably due to the formation of $Cd(OH)_2$ precipitation, which lowers the amount of free metal ions available for adsorption on the solid surface of the adsorbent.

On the other hand, the adsorption behavior of Pb(II) ions exhibits a distinct pattern. At pH 3, adsorption reaches its maximum, then steadily declines as pH rises. This can be explained by the solubility product (Ksp) values of the corresponding metal hydroxide, which are 7.5×10^{-15} and 1.2×10^{-15} for $Cd(OH)_2$ and $Pb(OH)_2$, respectively.

Since $Pb(OH)_2$ has a lower Ksp, it precipitates earlier than $Cd(OH)_2$. At pH 5, significant precipitation of $Pb(OH)_2$ likely occurs, while $Cd(OH)_2$ formation begins predominantly above pH 6. Therefore, the optimal pH for the adsorption of Cd(II) and Pb(II) was determined to be pH 4 and pH 3, respectively.

Adsorption kinetics study

The adsorption kinetics were studied using the following models: first-order, second-order, pseudo-first-order, and pseudo-second-order. **Figure 7** indicates that the adsorption of both Cd(II) and Pb(II) increased rapidly during the initial contact time, reaching near-equilibrium within a short duration. A substantial increase in adsorption capacity was observed during the initial 10 minutes. This phenomenon is attributed to the abundance of active sites on the adsorbent surface.

Following the initial uptake, the adsorption rate gradually decreased. The adsorption capacities for Cd(II) and Pb(II) exhibited minimal variation as contact time increased. This trend indicates that the majority of active sites became occupied, leading to a reduced migration rate of metal ions to the remaining available sites. The optimal contact time was determined to be 60 minutes, as both metal ions reached a stable adsorption capacity after this point.

Table 2 shows that the adsorption process of Cd(II) and Pb(II) ions on $Fe_3O_4@SiO_2@meso\text{-}SiO_2@TMPDT$ follows the pseudo-second-order kinetic model, with R^2 values closest to 1. The pseudo-second-order model assumes that the metal ions are adsorbed chemically through electron exchange or interaction between the metal ions and the adsorbent. Chemical adsorption, or chemisorption, occurs as metal ions bind to the adsorbent surface through the formation of complex bonds between the amine functional groups of TMPDT and the metal ions as the central atoms. The rate constant (k) represents the reaction rate, with higher k values indicating faster reaction rates. The highest k values were observed for Cd(II) ions (0.148 g mg^{-1} min^{-1}) compared to Pb(II) ions (0.096 g mg^{-1} min^{-1}). A higher adsorption rate constant implies a faster adsorption process.

The adsorption kinetic model can also be determined by comparing the calculated Q_e values with the experimental results, as shown in **Table 3**.

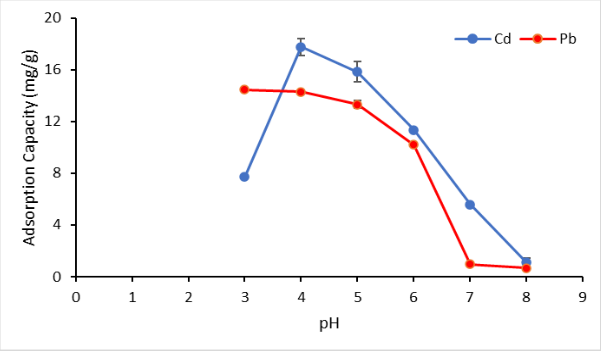

Figure 6. The effect of pH on adsorption capacity of Cd(II) and Pb(II)

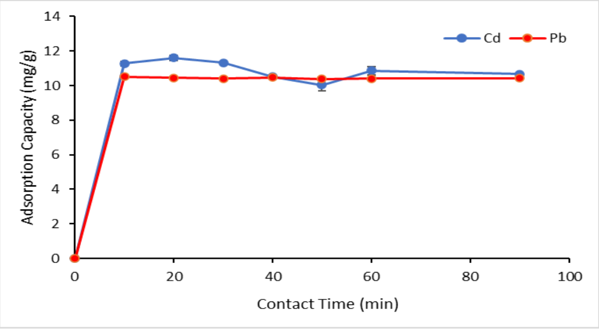

Figure 7. The effect of contact time on adsorption of Cd(II) and Pb(II)

Table 2. Kinetic model for Fe_3O_4@SiO_2@meso-SiO_2@TMPDT

Kinetic models	K		R^2	
	Cd(II)	Pb(II)	Cd(II)	Pb(II)
First-order	0.00186	0.0077	0.255	0.3575
Second-order	-0.0008	-0.0630	0.003	0.3789
Pseudo-first-order	0.025	0.035	0.371	0.1255
Pseudo-second-order	0.148	0.096	0.997	1.000

Table 3. Adsorption capacity at equilibrium Q_e

Kinetic models	Parameter	Q_e (mg/g)	
		Cd(II)	Pb(II)
	Experiment	10.66	10.46
Pseudo-first- order	Calculation	1.9873	1.9 x 10^{-6}
Pseudo-second-order	Calculation	10.54	10.40

The calculated $Q_e$values that most closely match the experimental values are those derived from the pseudo-second-order model, with the calculated values for Cd(II) and Pb(II) being 10.54 mg/g and 10.40 mg/g, respectively, while the experimental values were 10.66 mg/g and 10.46 mg/g. This further confirms that the adsorption kinetics of Cd(II) and Pb(II) ions using Fe_3O_4@SiO_2@meso-SiO_2@TMPDT follows the pseudo-second-order model.

Adsorption isotherm study

The type of adsorption isotherm is employed to determine the maximum adsorption capacity and to predict the nature of the interaction between the adsorbent and metal ions. The adsorption isotherm was determined by evaluating the coefficient of determination (R^2), with the model that exhibited the closest value to 1 being considered the best fit. The adsorption isotherm graph for Fe_3O_4@SiO_2@meso-SiO_2@TMPDT toward Cd(II) and Pb(II) ions is presented in **Figure 8.**

Table 4 shows that the R^2 values for both the Langmuir and Freundlich isotherms for Cd(II) and Pb(II) are quite similar, suggesting that the adsorption process of Cd(II) and Pb(II) using Fe_3O_4@SiO_2@meso-SiO_2@TMPDT occurs through both chemical and physical interactions. The chemisorption process occurs due to the active groups on the adsorbent, specifically the amine groups on the adsorbent surface, which possess lone electron pairs that bind to the positively charged Cd(II) and Pb(II) metal ions. Physical interactions, on the other hand, occur through the silica pores in the adsorbent.

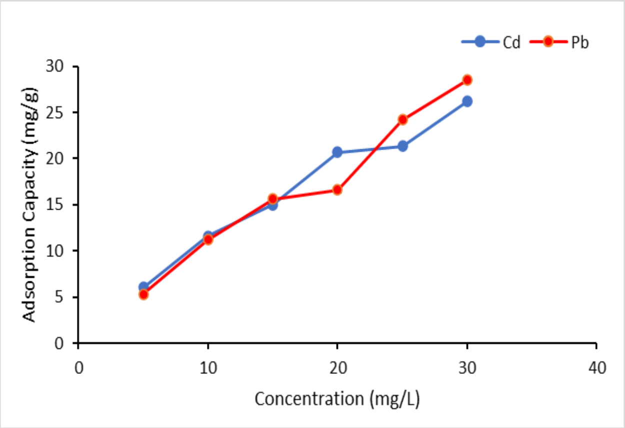

Figure 8. The effect of concentration on adsorption capacity

Table 4. Adsorption isotherm model

Adsorption isotherm models	Fe_3O_4@SiO_2@meso-SiO_2@TMPDT	
	Cd(II)	Pb(II)
Langmuir		
Q_m (mg/g)	28.089	24.498
R_L	0.198	0.077
R^2	0.898	0.729
Freundlich k_f (mg/g)	10.668	29.291
n	2.417	1.777
R^2	0.878	0.755

The maximum adsorption capacity (Q_m) indicates that a higher value reflects a greater ability of the adsorbent to retain the adsorbate. The maximum capacity for Cd(II) is greater than for Pb(II), with values of 28.089 mg/g and 24.498 mg/g, respectively.

This can be explained by several factors: (1) Ion Size and Electron Configuration: Cd(II) has a smaller ionic radius (approximately 0.95 Å) and its valence electrons are closer to the nucleus, making Cd(II) more prone to forming stronger bonds with smaller and denser ligands. In contrast, Pb(II) has a larger ionic radius (approximately 1.19 Å), leading to weaker bonding with ligands such as amines. (2) Complex Stability and Ligand Characteristics: As a transition metal, Cd(II) tends to form more stable complexes with amine groups. This is due to its tendency to form more organized and stable complexes with a high affinity for electron-donating groups like amines. On the other hand, Pb(II) is not a transition metal, and thus the complex formation with amine groups is weaker. (3) Reaction Rate Constant (k): Based on pseudo-second-order kinetics, Cd(II) exhibits a higher rate constant (k = 0.148), indicating faster adsorption on the adsorbent. In contrast, Pb(II) has a smaller rate constant (k = 0.096), leading to slower adsorption.

The R_L value indicates whether the adsorption process is favorable. An R_L value greater than 1 indicates an unfavorable process, $R_L = 1$ is linear, $0 < R_L < 1$ indicates a favorable process, and $R_L = 0$ indicates irreversible adsorption. For Cd(II) and Pb(II) adsorption, the R_L values are between 0 and 1, indicating that the process is favorable. This is further supported by the Freundlich isotherm data, where the intensity index (n) is greater than 1, confirming that the adsorption process is advantageous.

The adsorption mechanism of Fe_3O_4@SiO_2@meso-SiO_2@TMPDT towards Cd(II) and Pb(II) is provided in **Figure 9.** The adsorption of divalent metal ions (M^{2+}, e.g. Cd^{2+} or Pb^{2+}) on the Fe_3O_4@SiO_2@meso-SiO_2@TMPDT adsorbent occurs mainly through a surface complexation mechanism between the donor nitrogen atom in the amine group of the TMPDT ligand and the metal ion in solution. The initially hydrated M^{2+} ion diffuses to the mesoporous silica surface, then some of the water molecules in the hydration shell are replaced by lone electron pairs on N ($-NH_2$/$-NH-$), forming a stable coordination bond. Because TMPDT has several N atoms, the binding is generally multidentate (chelate effect) thereby increasing the bond strength. The presence of mesopores increases the surface area and facilitates ion access to the active site, while the Fe_3O_4 core plays a major role as a magnetic separation without becoming a dominant bonding center.

For comparison, the $Q_m$values of various adsorbents are presented in **Table 5**. The Q_m value for the Fe_3O_4@SiO_2@meso-SiO_2@TMPDT adsorbent is higher, even when compared to Fe_3O_4@SiO_2-TMPDT adsorbents previously studied by the other authors. This indicates that the addition of mesoporous silica enhances the adsorption capacity of the adsorbent.

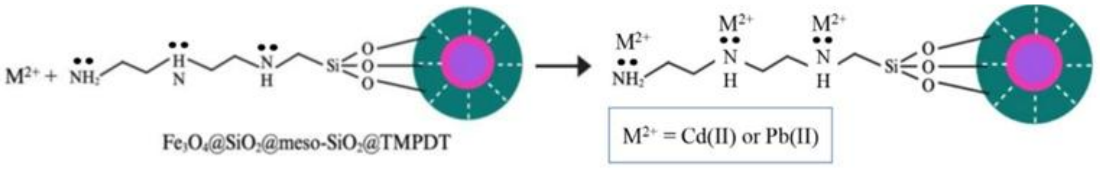

Figure 9. Proposed adsorption mechanism of Cd(II) and Pb(II) onto Fe_3O_4@SiO_2@meso-SiO_2@TMPDT

Table 5. The comparison of maximum adsorption capacity of other adsorbents with Fe_3O_4@SiO_2-TMPDT

Material	Adsorbate	Q_m (mg/g)	References
Fe_3O_4@SiO_2@meso- SiO_2@TMPDT	Pb(II)	24.498	This work
Fe_3O_4@SiO_2@meso- SiO_2@TMPDT	Cd(II)	28.089	This work
Fe_3O_4@SiO_2-TMPDT	Pb(II)	11.760	(Hastuti et al., 2025)
Fe_3O_4@SiO_2-TMPDT	Cd(II)	1.888	(Hastuti et al., 2025)
Silica@mercapto (HS@M)	Pb(II)	4.97	(Naat et al., 2021)
Rice husk	Cd(II)	5.13	(Montalvo-Andía et al., 2022)

CONCLUSIONS

The characterization of the adsorbent by FTIR, SEM-EDX, and TGA confirmed the successful synthesis of magnetized and TMPDT-functionalized silica derived from rice husk ash. The developed adsorbent exhibited effective removal of Cd(II) and Pb(II) under optimal conditions, with maximum adsorption capacities for Cd(II) and Pb(II) were 28.089 mg/g and 24.498 mg/g, respectively, demonstrating competitive performance compared to previous reported adsorbents. The adsorption kinetics for both metal ions followed a pseudo-second-order model. Furthermore, the adsorption isotherms fit both the Langmuir and Freundlich models with comparable coefficients of determination (R^2), suggesting that adsorption occurred on a heterogeneous surface involving both monolayer and multilayer interactions. The incorporation of a magnetic Fe_3O_4 core enables facile separation of the adsorbent from aqueous media, highlighting its practical potential for efficient and sustainable heavy metal removal.

ACKNOWLEDGEMENTS

The authors would like to express their sincere gratitude to Sebelas Maret University for their invaluable support and assistance in conducting this research. Special thanks are also due to the Research Groups Grant (No 194.2/UN27.22/PT.01.03/2024) for funding this study and to all those who contributed to the success of this work.

REFERENCES

Amaria, Suyanta, & Nuryono. (2017). Coating of L-arginine modified silica on magnetite through two different sol-gel routes. *Indonesian Journal of Chemical*, *17*(2), 256–263. https://doi.org/10.22146/ijc.23642.

Awual, M. R., Hasan, M. M., & Shahat, A. (2014). Functionalized novel mesoporous adsorbent for selective lead(II) ions monitoring and removal from wastewater. *Sensors and Actuators, B: Chemical*, *203*, 854–863. https://doi.org/10.1016/j.snb.2014.07.063.

Beagan, A., Alotaibi, K., Almakhlafi, M., Algarabli, W., Alajmi, N., Alanazi, M., Alwaalah, H., Alharbi, F., Alshammari, R., & Alswieleh, A. (2022). Amine and sulfonic acid functionalized mesoporous silica as an effective adsorbent for removal of methylene blue from contaminated water. *Journal of King Saud University - Science*, *34*(2), 101762. https://doi.org/10.1016/j.jksus.2021.101762.

Bouafia, A., Laouini, S. E., Tedjani, M. L., Ali, G. A. M., & Barhoum, A. (2022). Green biosynthesis and physicochemical characterization of Fe_3O_4 nanoparticles using Punica granatum L. fruit peel extract for optoelectronic applications. *Textile Research Journal*, *92*(15–16), 2685–2696. https://doi.org/10.1177/00405175211006671.

Chan, C. C. P., Choudhury, N. R., & Majewski, P. (2011). Fabrication and characterisation of self-assembled monolayers of N-[3-(trimethoxysilyl)propyl]diethylenetriamine on silica particles. *Colloids and Surfaces A: Physicochemical and Engineering Aspects*, *377*(1–3), 20–27. https://doi.org/10.1016/j.colsurfa.2010.12.003.

Cheng, Q., Luo, E., Gan, L., Luo, W., Luo, X., Wan, S., & Li, S. (2025). Construction of quaternary ammonium nitroxy-hybrid magnetic mesoporous silica adsorbent system and its selective adsorption research of Re(Ⅶ)/Cu(Ⅱ). *Separation and Purification Technology*, *354*, 129181. https://doi.org/10.1016/J.SEPPUR.2024.129181.

El-Said, A. G., Badawy, N. A., & Garamon, S. E. (2018). Adsorption of heavy metal ions from aqueous solutions onto rice husk ash low cost adsorbent. *Journal of Environmental &*

Analytical Toxicology, *08*(01). https://doi.org/10.4172/2161-0525.1000543.

Fahmiati, Nuryono, & Suyanta. (2018). Functionalization of silica coated on iron sand magnetic material with diethylenetriamine. *Asian Journal of Chemistry*, *30*(8), 1805–1810. https://doi.org/10.14233/ajchem.2018.21314.

Fitriana, D., Mudasir, M., & Siswanta, D. (2025). The Modification of coal fly ash adsorbent using dithizone immobilization for Cd(II) ions removal. *Jurnal Kimia Sains dan Aplikasi, 28*(4), 215–224. https://doi.org/10.14710/jksa.28.4.215-224.

Hastuti, S., Martini, T., Wibowo, A. H., Fitriana, D., Zuhara, W., Mutma'inah, H., & Putri, R. I. (2025). Removal of heavy metals: Pb(II), Ni(II) And Cd(II) By Fe_3O_4@SiO_2-TMPDT adsorbent prepared from rice husk ash. *ALCHEMY Jurnal Penelitian Kimia*, *21*(1), 53. https://doi.org/10.20961/alchemy.21.1.91934.53-63.

Hastuti, S., Nuryono, & Kuncaka, A. (2019). Synthesis and characterization of L-Arginine modified silica by sol-gel method prepared rice hull ash. *IOP Conference Series: Materials Science and Engineering*, *509*(1) 012135. https://doi.org/10.1088/1757-899X/509/1/012135.

He, H., Ye, S., Zhang, W., Li, S., Nie, Z., Xu, X., Li, W., Abdukayum, A., Chen, W. T., & Hu, G. (2024). Synthesis of magnetic mesoporous silica adsorbents by thiol-ene click chemistry with optimised lewis base properties through molecular imprinting for the rapid and effective capture of Pb(II). *Chemical Engineering Journal*, *489*, 151294. https://doi.org/10.1016/J.CEJ.2024.151294.

Husain, H., Hariyanto, B., Sulthonul, M., Klysubun, W., Darminto, D., & Pratapa, S. (2019). Structure and magnetic properties of silica-coated magnetite- nanoparticle composites. *Materials Research Express*, *6*, 086117. https://doi.org/10.1088/2053-1591/ab29af.

Javaheri, F., Kheshti, Z., Ghasemi, S., & Altaee, A. (2019). Enhancement of Cd^{2+} removal from aqueous solution by multifunctional mesoporous silica: Equilibrium isotherms and kinetics study. *Separation and Purification Technology*, *224*, 199–208. https://doi.org/10.1016/j.seppur.2019.05.017.

Jiaqi, Z., Yimin, D., Danyang, L., Shengyun, W., Liling, Z., & Yi, Z. (2019). Synthesis of carboxyl-functionalized magnetic nanoparticle for the removal of methylene blue. *Colloids and Surfaces A: Physicochemical and Engineering Aspects*, *572*, 58–66. https://doi.org/10.1016/j.colsurfa.2019.03.095.

Kheshti, Z., Ghajar Azodi, K., Altaee, A., & Kheshti, M. R. (2019). High-gradient magnetic separator (HGMS) combined with adsorption for nitrate removal from aqueous solution. *Separation and Purification Technology*, *212*, 650–659. https://doi.org/10.1016/j.seppur.2018.11.080.

Kheshti, Z., & Hassanajili, S. (2017). Novel multifunctional mesoporous microsphere with high surface area for removal of zinc ion from aqueous solution: Preparation and characterization. *Journal of Inorganic and Organometallic Polymers and Materials*, *27*(6), 1613–1626. https://doi.org/10.1007/s10904-017-0621-x.

Kimia Sains dan Aplikasi, J., Fitriana, D., & Siswanta, D. (2025). The modification of coal fly ash adsorbent using dithizone immobilization for Cd(II) ions removal. *Jurnal Kimia Sains Dan Aplikasi*, *28*(4), 215–224. https://doi.org/10.14710/jksa.28.4.215-224.

Larkunthod, P., Boonlakhorn, J., Pansarakham, P., Pongdontri, P., Thongbai, P., & Theerakulpisut, P. (2022). Synthesis and characterization of silica nanoparticles from rice husk and their effects on physiology of rice under salt stress. *Chilean Journal of Agricultural Research*, *82*(3), 412–425. https://doi.org/10.4067/S0718-58392022000300412.

Liu, Y., Fu, R., Sun, Y., Zhou, X., Baig, S. A., & Xu, X. (2016). Multifunctional Nanocomposites Fe_3O_4@SiO_2-EDTA for Pb(II) and Cu(II) removal from aqueous solutions. *Applied Surface Science*, *369*, 267–276. https://doi.org/10.1016/j.apsusc.2016.02.043.

Martini, T., Hastuti, S., Aliestyani, R. M., & Azzahra, P. (2024). Synthesis of silica-based imprinted ionic from rice husk ash for adsorption of Ni(II). *Key Engineering Materials*, *990*, 51–58.

Mayoral, A., Blanco, R. M., & Diaz, I. (2013). Location of enzyme in lipase-SBA-12 hybrid biocatalyst. *Journal of Molecular Catalysis B: Enzymatic*, *90*, 23–25. https://doi.org/10.1016/j.molcatb.2013.01.012.

Meng, L., Chan, Y., Wang, H., Dai, Y., Wang, X., & Zou, J. (2016). Recycling of iron and silicon from drinking water treatment sludge for synthesis of magnetic iron oxide@SiO_2 composites. *Environmental Science and Pollution Research*, *23*(6), 5122–5133. https://doi.org/10.1007/S11356-015-5742-6.

Montalvo-Andía, J., Reátegui-Romero, W., Peña-Contreras, A. D., Zaldivar Alvarez, W. F., King-Santos, M. E., Fernández-Guzmán, V., Guerrero-Guevara, J. L., & Puris-Naupay, J. E. (2022). Adsorption of Cd (II) using chemically modified rice husk: characterization, equilibrium, and kinetic studies. *Adsorption Science and Technology*, *2022*, 17. https://doi.org/10.1155/2022/3688155.

Naat, J. N., Neolaka, Y. A. B., Lapailaka, T., Tj, R. T., Sabarudin, A., Darmokoesoemo, H., & Kusuma, H. S. (2021). Adsorption of Cu(II) and Pb(II) using silica@mercapto (hs@m) hybrid adsorbent synthesized from silica of takari sand: optimization of parameters and kinetics. *Rasayan Journal of Chemistry*, *14*(1), 550–560. https://doi.org/10.31788/RJC.2021.1415803.

Priya, A. K., Yogeshwaran, V., Rajendran, S., Hoang, T. K. A., Soto-Moscoso, M., Ghfar, A. A., & Bathula, C. (2022). Investigation of mechanism of heavy metals (Cr^{6+}, Pb^{2+}& Zn^{2+}) adsorption from aqueous medium using rice husk ash: Kinetic and thermodynamic approach. *Chemosphere*, *286*, 131796. https://doi.org/10.1016/J.CHEMOSPHERE.2021.131796.

Ripon, R. I., Begum, Z. A., Miyazawa, R., Leonard, K., Ogata, M., Ahmmad, B., & Rahman, I. M. M. (2024). Development and application of a new macrocyclic ligand-functionalized mesoporous silica sorbent for selective separation of radiocesium from environmental wastewater. *Microchemical Journal*, *207*, 111649. https://doi.org/10.1016/J.MICROC.2024.111649.

Sakti, S. C. W., Siswanta, D., & Nuryono. (2013). Adsorption of gold(III) on ionic imprinted amino-silica hybrid prepared from rice hull ash. *Pure and Applied Chemistry*, *85*(1), 211–223. https://doi.org/10.1351/PAC-CON-12-01-02.

Sanati, A. M., Kamari, S., & Ghorbani, F. (2019). Application of response surface methodology for optimization of cadmium adsorption from aqueous solutions by Fe_3O_4@SiO_2@APTMS core–shell magnetic nanohybrid. *Surfaces and Interfaces*, *17*. https://doi.org/10.1016/j.surfin.2019.100374.

Yu, W., Lan, H., Wu, Z., Pan, D., & Wu, Y. (2025). Enhanced selective extraction of biogenic amines using carboxyl-functionalized SBA-15 and SBA-16 mesoporous silica. *Microporous and Mesoporous Materials*, *382*, 113404. https://doi.org/10.1016/J.MICROMESO.2024.113404.

Zhan, Y., Luo, X., Nie, S., Huang, Y., Tu, X., & Luo, S. (2011). Selective separation of Cu(II) from aqueous solution with a novel Cu(II) surface magnetic ion-imprinted polymer. *Industrial and Engineering Chemistry Research*, *50*(10), 6355–6361. https://doi.org/10.1021/ie102177e.

Zhou, J., Zhou, X., Yang, K., Cao, Z., Wang, Z., Zhou, C., Baig, S. A., & Xu, X. (2020). Adsorption behavior and mechanism of arsenic on mesoporous silica modified by iron-manganese binary oxide (FeMnOx/SBA-15) from aqueous systems. *Journal of Hazardous Materials*, *384*. https://doi.org/10.1016/j.jhazmat.2019.121229.